Quaternary Science Reviews 270 (2021) 107171

Contents lists available at ScienceDirect

Quaternary Science Reviews

journal homepage: www.elsevier.com/locate/quascirev

Centennial scale climate oscillations from southern Siberia in the Last Glacial Maximum

Vadim A. Kravchinsky [a, b], Rui Zhang [a, b, *], Ryan Borowiecki [b], Pavel E. Tarasov [c], Mirko van der Baan [b], Taslima Anwar [a, b], Avto Goguitchaichvili [d], Stefanie Müller [c]

[a] Institute of Cenozoic Geology and Environment, State Key Laboratory of Continental Dynamics, Department of Geology, Northwest University, Xi'an, 710069, China
[b] Geophysics, Department of Physics, University of Alberta, Edmonton, Alberta, T6G2E1, Canada
[c] Institute of Geological Sciences, Palaeontology, Freie Universitaet Berlin, Malteserstraße 74-100, Building D, 12249, Berlin, Germany
[d] Servicio Arqueomagnético Nacional, Instituto de Geofísica, UNAM, Unidad Michoacán, Campus Morelia, Michoacán, Mexico

ARTICLE INFO

Article history:
Received 28 March 2021
Received in revised form
16 August 2021
Accepted 26 August 2021
Available online xxx

Handling Editor: Dr C. O'Cofaigh

Keywords:
Climate change
Continental climate
Holocene
Last glacial maximum
Pollen concentration
Spectral analysis

ABSTRACT

A lack of adequate high resolution climate proxy records for the Last Glacial Maximum (LGM) has prevented the extrapolation of climate–solar linkages on centennial time scales prior of the Holocene. Therefore, it is still unknown whether centennial climate variations of the last ten thousand years convey a universal climate change or merely represent a characteristic of the Holocene. Recently published high resolution climate proxy records for the LGM allowed us to extrapolate climate–solar linkages on centennial time scales ahead of the Holocene. Here we present the analysis of a high resolution pollen concentration record from Lake Kotokel in southern Siberia, Russia, during the LGM. The record reflects the dynamics of vegetation zones and temperature change with a resolution of ~40 years in the continental climate of north-eastern Asia. We demonstrate that our pollen concentration record, the oxygen isotope $\delta^{18}O$ record from the Greenland ice core project NGRIP (NorthGRIP), the dust-fall contributions in Lake Qinghai, China, grain size in the Gulang and Jingyuan loess deposits, China, and the composite oxygen isotope $\delta^{18}O$ record from the Alpine cave system 7H reveal cooler to warmer climate fluctuations between ~ 20.6 and 26 ka. Such fluctuations correspond to the ~1000-yr, 500-600-yr and 210-250-yr cycles possibly linked to the solar activity variations and recognized in high resolution Holocene proxies all over the world. We further show that climate fluctuations in the LGM and Holocene are spectrally similar suggesting that linkages between climate proxies and solar activity at the centennial time scale in the Holocene can be extended to the LGM.

1. Introduction

Centennial to millennial scale climate oscillations in the Holocene Epoch, the current interglacial period, have been reported on continents and in the ocean in each climate zone and extensively reviewed (Soon et al., 2014; Marsicek et al., 2018; Wanner et al., 2008). Observed Holocene temperature fluctuations have amplitudes greater than 1 °C (McMichael, 2012). Meanwhile, the centennial scale climate variability remains poorly identified during the Last Glacial Maximum (LGM), defined between ~ 26.5 and 20 ka in Clark et al. (2009), because the data typically lack sufficient temporal resolution. To address this, our study analyses a high resolution continental climate record between ~26 and 20.6 ka during the LGM, when ice sheets were at their maximum extent as a result of reduced northern summer insolation, tropical Pacific sea surface temperatures, and atmospheric carbon dioxide (Clark et al., 2009).

Spectral analyses of Holocene climate proxy records from different parts of the world revealed persistent periodicities of ~2300–2500, ~1000, ~700 and ≤ 500 years that is often interpreted

* Corresponding author. Institute of Cenozoic Geology and Environment, State Key Laboratory of Continental Dynamics, Department of Geology, Northwest University, Xi'an, 710069, China.
E-mail address: ruizhang@nwu.edu.cn (R. Zhang).

https://doi.org/10.1016/j.quascirev.2021.107171
0277-3791/

as an indication of variations in solar activity during the Holocene (Debret et al., 2009; Soon et al., 2014; Marsicek et al., 2018; Wanner et al., 2008). Power spectra of the solar activity reconstructed from ^{10}Be and ^{14}C in the GRIP ice core (Vonmoos et al., 2006) show distinct peaks around 700, 500 and 350 yr, as well as the well-known 210 yr peak (Suess or de Vries cycle) in the last 6 kyrs (Wanner et al., 2008). Analysis of a combination of different ^{10}Be ice core records from Greenland and Antarctica with the global ^{14}C tree ring record demonstrated presence of significant periodicities at 210, 350 and 1000 yr and less significant cycles at ~500 and 710 yr that are also found in some Asian climate records (Steinhilber et al., 2012).

An earlier reported ~1500-yr Bond cycle corresponding to North Atlantic oceanic circulation (Bond et al., 1997; Bianchi and McCave, 1999; Loehle and Singer, 2010) may have widespread global distribution, but only in the late Holocene (Debret et al., 2009). The 1500-yr cycle was reported to dominate the Greenland ice core record and some deep sea cores (Wunsch, 2000; Schulz, 2002). Dima and Lohmann (2009) suggested that the internal threshold response of the thermohaline circulation (THC) to solar forcing is more likely to produce the observed 1500-yr periodicity. The leading explanation of rapid climate fluctuations is cooling and freshening of the North Atlantic by an influx of freshwater (Bond et al., 1999). Rapid climate fluctuations during the early Holocene are explained to be related to feedback mechanisms linked to amplified changes in the amount of solar radiation with the ~1000-yr cyclicity with internal climate system variability with the ~1500-yr cyclicity being important for the second half of the Holocene (Debret et al., 2009). Different feedback mechanisms have been suggested to amplify the centennial scale climate changes caused by solar activity (Gray et al., 2010). The suggested feedback mechanisms include changes in the zonal equatorial and meridional circulations (Walker and Hadley circulations), cloud increase and decrease of solar radiation, direct total solar irradiance increase and decrease over relatively cloud-free subtropical oceans, stratospheric ozone changes, planetary wave propagation when the wind anomaly moves poleward and downward with time and grows significantly in amplitude, stratosphere and troposphere coupling, centennial scale irradiance variations, and changes in energetic particle fluxes. At the same time the 1500-yr cycle observed in the North Atlantic circulation during the last 6.5 kyr is suggested to be of non-solar origin connecting the cycle to internal variability with distinct periods of storminess (Sorrel et al., 2012). The reconstructions of the Holocene sea-ice drift record in the Arctic showed a strong 1500-yr cycle that does not match the spectral characteristics of solar-forcing records suggesting that the circulation patterns in the Arctic Ocean on millennial timescales are not influenced by the solar forcing (Darby et al., 2012). However, the study of the lake sediments in Central Germany suggested that periods of increased storminess occur when solar activity is lowest and solar variability may be influencing climatic changes (Martin-Puertas et al., 2012). All these studies demonstrate that various forcing mechanisms and periodicities may co-exist in the Holocene and different regions may be impacted differently by the combination or domination of some or all of these mechanisms.

Some studies consider that Dansgaard-Oeschger (DO) events (rapid climate fluctuations during the last glacial period) are quasi-periodic (Grootes and Stuiver, 1997) and are separated by intervals with multiples of ~1470 years (Rahmstorf, 2003). Such oscillations resemble the Holocene Bond cyclicity (ice rafting events that are linked to climate fluctuations), however, the absence of a regular signal when only multiples are present, is hard to explain. Pisias et al. (2010) obtained the spectral power mode at ~1600 yr when analysing 38 paleoclimatic records from different parts of the world in the interval of 60–26 ka. Contrary to Rahmstorf (2003) they interpreted such periodicity to be associated with changes internal to the climate system. Long and Stoy (2013) reported that the millennial-scale periodicities in the oxygen isotope records of the Greenland Ice Sheet Project 2, North Greenland Ice Core Project (NGRIP) and sea-surface temperature derived from the Bermuda Rise sedimentary core vary depending on the observational time interval. Some studies, however, showed that a possibility of random event generation for the DO cycles cannot be statistically rejected (Schulz, 2002; Ditlevsen et al., 2007; Peavoy and Franzke, 2010).

The Holocene periodicities of 1000-yr and 500-yr are already shown in the climatic proxy series of the Lake Baikal area and compared to the solar activity variance and sunspot number (Kravchinsky et al., 2013). In our current study we analysed LGM climate records to find out if similar centennial periodicities persisted during the 26 and 20.6 ka in the same Lake Baikal region. The reconstructions of the solar variations on the centennial timescale are available for the Holocene, not for the LGM, therefore analysis of the high-resolution climate proxies plays the leading role in revealing persistent Sun–climate links before the Holocene. It was shown that solar minima correlate with more negative δ^{18}O values in the Greenland ice record on the centennial timescale (150–500 yr) suggesting the existence of strong solar forcing on the climate between 22.9 and 14.7 ka (Adolphi et al., 2014). The ~2300–2500 yr cycle in the Holocene appears to be the Hallstatt cycle related to the solar activity variations (Usoskin et al., 2007) or to a major resonance involving the movements of the four Jovian planets that changes the cosmic ray and dust densities in the inner region of the solar system modulating the radionucleotide production and influencing climate through a cloud modulation (Scafetta et al., 2016).

Our data were obtained from the continuous sedimentary record of the Lake Kotokel sediment core KTK10/6, east of Lake Baikal (Fig. 1) (drilling site at 52°47.276′N, 108°07.435′E). Müller et al. (2014) reported a pollen percentage and a linear age model from the previous study of Bezrukova et al. (2010) in order to evaluate the environmental stability of the region for a large population of herbivores. They demonstrated that the LGM environment of the Lake Baikal region was favourable for inhabiting by hunter–gatherer groups. In this study we report and make public higher resolution results of the pollen analysis comparing to Müller et al. (2014) in order to evaluate centennial scale climate variations. We also present a new nonlinear age model using seven accelerator mass spectrometry (AMS) radiocarbon (^{14}C) dates from the sediment core KTK10/6 reported. Tentative linear age model was used in Müller et al. (2014) that worked well for describing long-term features but cannot be used for centennial scale event determination. The core was collected from a site in the southern part of Lake Kotokel (Fig. 1c). In this study we present the detailed total pollen concentration (TPC) and percentage of *Cyperaceae* and *Artemisia*, two types of plants, as these parameters occur in the greatest abundance in Lake Kotokel and depend directly on the humidity conditions in the region.

The Lake Kotokel drainage basin is situated in the area of forest-steppe and steppe ecosystems that are highly sensitive to climatic changes created by the interaction of the three largest systems of atmospheric circulation: Siberian Anticyclone, Westerlies, and Pacific monsoon (Bezrukova et al., 2010, 2011). Dry, cold and sunny winter weather is associated with the Siberian Anticyclone centered at ~50°N/100°E. The Anticyclone has a direct influence on the surface air temperature and the Pacific winter monsoon routes (Gong et al., 2001; Panagiotopoulos et al., 2005). The westerly wind from the Atlantic dominates through the year and transports

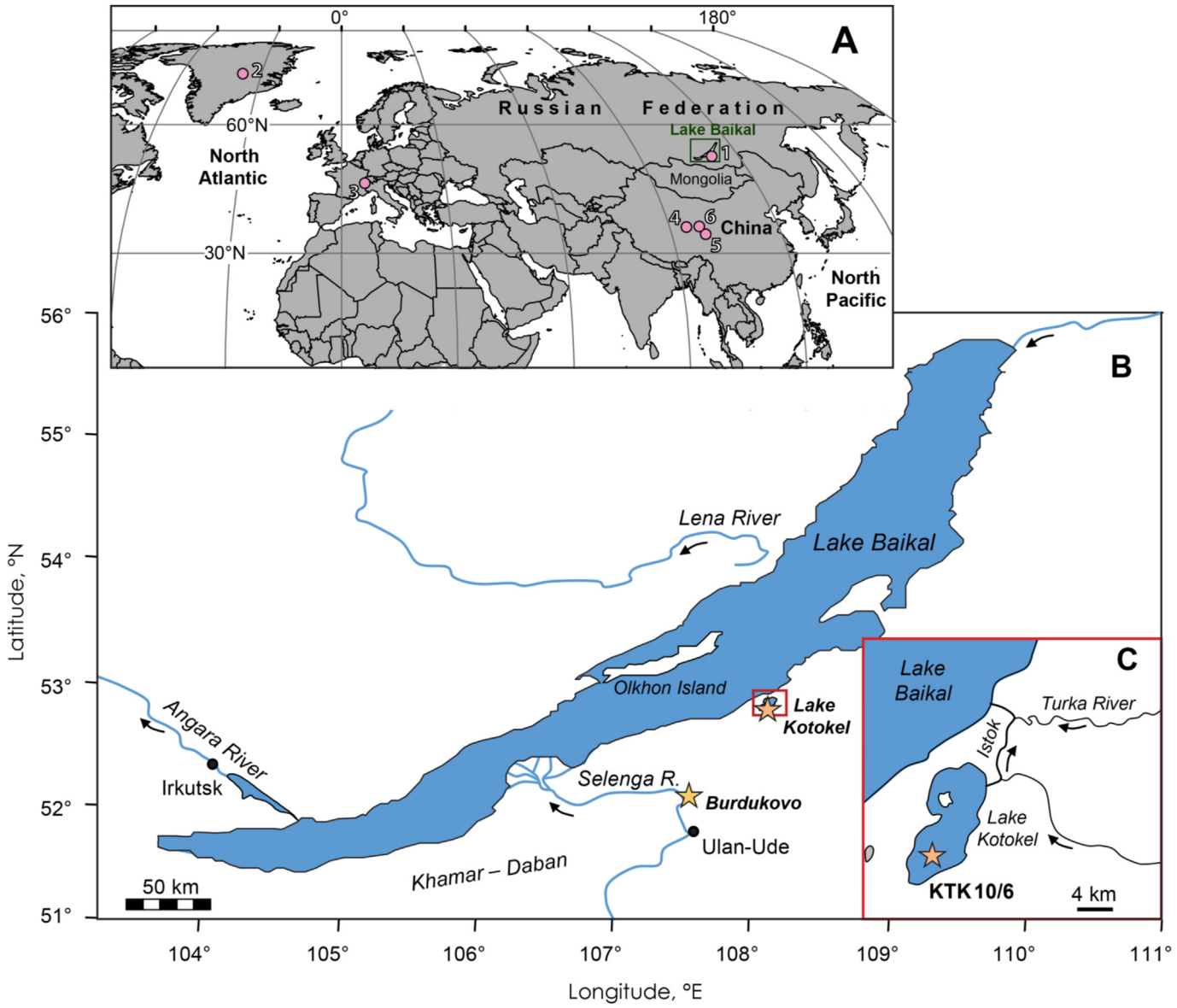

Fig. 1. Geographic location of the study region and other sections used for comparison (A); location of the Lake Kotokel coring site and the Burdokovo loess-soil section site (Kravchinsky et al., 2013) (B); close-up of the coring site location in Lake Kotokel (C). The records compared in this study: (1) Lake Kotokel (this study), (2) the oxygen isotope $\delta^{18}O$ record from the Greenland ice core project (NGRIP) (Rasmussen et al., 2014), (3) the composite oxygen isotope $\delta^{18}O$ record from the Alpine cave system 7H (Luetscher et al., 2015), (4) dust-fall contributions in Lake Qinghai in China (An et al., 2012), (5) grain size at the Jingyuan, and (6) Gulang loess sections in China (Sun et al., 2012).

precipitation during autumn and spring, weakening in the summer when warm and wet Pacific air bringing heavy rainfall to the region (Bezrukova et al., 2008, 2010).

The palynology studies of the Lake Kotokel core sediments already demonstrated that the timing and succession of major climatic events in the Kotokel record corresponded to all climatic events registered previously at other lakes in the region including Lake Baikal at mid-latitudes of Eurasia (Tarasov et al., 2005; Shichi et al., 2009; Bezrukova et al., 2008, 2010, 2011; Müller et al., 2014). The sediments record Marine Isotope Stages 1–3, the Younger Dryas, LGM and smaller scale climatic events. Total pollen count (grains/g) and biome scores for steppe and taiga were used in these studies as paleoclimatic indicators in the Lake Kotokel and Lake Baikal region. Synchronism of short-term climatic fluctuations in the Lake Kotokel and Lake Baikal area with global fluctuations revealed that the pollen analysis provides an excellent climate proxy that was confirmed with geochemistry, diatom analysis and oxygen isotope studies (Tarasov et al., 2009; Kostrova et al., 2016). A redistribution of the atmospheric moisture balance was suggested as a possible mechanism behind rhythmic variations in the environment of the southern part of East Siberia and the Lake Kotokel (Bezrukova et al., 2008, 2010, 2011; Tarasov et al., 2009; Shichi et al., 2009; Müller et al., 2014), therefore variations in pollen concentration were used as a climate proxy to evaluate relative moisture changes. To reconstruct centennial scale climate fluctuations during the LGM and compare them with available global records, we analysed a high resolution time series of total pollen concentrations in Lake Kotokel. *Artemisia* (e.g. wormwood, sagebrush, etc.), *Poaceae* (grasses), and *Cyperaceae* (sedges) comprised up to 90% of the pollen in the sediments (Müller et al., 2014), which together with a rich variety of other herbaceous taxa indicates productive vegetation during the LGM. The pollen and non-pollen palynomorph

assemblage representing the LGM interval is described in Müller et al. (2014). Low percentages of boreal tree and shrub pollen taxa demonstrate an absence of cold deciduous forest biome in the record and imply that the LGM climate was generally colder and drier than today's climate. There is no evidence that the LGM climate was desertic, as pollen percentages of *Chenopodiaceae* and *Ephedra* – taxa typical in the arid inner Asia – were very low (Müller et al., 2014).

2. Methods

2.1. Sampling, accelerator mass spectrometry (AMS) dating and pollen concentration analysis

The length of the undisturbed KTK10/6 core section was 190 cm (the depth of the core top was 970 cm). The sampling and lithological description was done on the working half of the core in the Institute of Geochemistry (Russian Academy of Sciences, Irkutsk). The top and middle parts of the KTK10/6 core consist of dense homogenous dark grey slightly laminated silty clay which becomes greenish dark grey in the bottom part of the KTK10/6 core. The half core was cut into 1 cm slices, packed in plastic containers and transported to the Free University (Berlin) for further analyses. The core has undisturbed organic mud through the whole length; it was sampled for the AMS radiocarbon ^{14}C dating. The dating was performed in the Poznan Radiocarbon Laboratory (Poland). The age spans of pollen and non-pollen palynomorph (NPP) records, based on seven AMS radiocarbon (^{14}C) dates, extended from 20.6 to 26 ka and thus covered the Last Glacial Maximum (LGM) in the definition of Clark et al. (2009).

To build a reliable age model based on the available AMS radiocarbon dates we used the Bayesian statistics approach based on controlling core accumulation rates utilizing a gamma autoregressive semiparametric model (Blaauw and Christen, 2011). Instead of linear interpolation between the average ages that assumes that there was constant sedimentation rate in between, the Bacon algorithm divides a core into many small sections and via Markov Chain Monte Carlo analysis estimates the sedimentation rate for each of these sections independently. In recent years the method has been extensively used to construct age models for the lake and peat sediments (e.g., Blaauw et al., 2018; Kaufman et al., 2020). The approach is particularly effective for high-density dated cores but also provides reasonable results in low-density dated cores.

In this study we constructed a new age model for the Lake Kotokel sediments that differs from the original linear age model in Müller et al. (2014) which was based in turn on the age model of Bezrukova et al. (2010). We used the seven radiocarbon dates obtained from an analysed segment of the KTK10/6 core (Fig. 2, Table 1). The AMS dates were used as the input for the Bacon software developed by Blaauw and Christen (2011) to construct a robust nonlinear age model. In addition to the absolute dates from both cores, the Bacon software utilizes the expected accumulation rate for lacustrine sediment and allowable rate of change of sediment accumulation ("memory" in the software). The approach uses these inputs to construct a non-gaussian autoregressive model for sediment accumulation which is informed by *a priori* knowledge of typical accumulation rates. Information on accumulation rates of Lake Kotokel in the Holocene and LGM is still scarce, therefore we used sedimentation rates for a similar age interval in records from the neighbouring Lake Baikal (Tarasov et al., 2005) and Lake Baunt (Solotchin et al., 2020) to make a preliminary estimate of 30 cm/kyr and use this value as initial input in Bacon software. An age model was then modified to better fit the actual age/depth record. We maintained the default 5 cm thickness for the cores in order to treat each age/depth pair as a point observation.

Upon comparison to the original age model developed by Müller et al. (2014), the dates for the samples are all shifted slightly older temporally, but the slope remains largely the same indicating there is no significant difference in sediment accumulation rates, and these rates fall well within those expected for lacustrine sediments in this region (Tarasov et al., 2005; Solotchin et al., 2020). Final calibrated age results using the Bayesian statistics approach from the Bacon software, that uses the calibration curve IntCal20 (Reimer et al., 2020), show that the mean 95% confidence interval width is 857 yr with 71% of dates intersecting the 95% confidence interval for the age model (Fig. 3). The core section comprises homogeneous, laminated, grey silty clay without any microscopic signatures of sediment composition change or bioturbation that repudiate a possibility of sudden fluctuations or reversals in sedimentation rate (Bezrukova et al., 2010; Müller et al., 2014). Therefore based on the Bayesian statistics approach result we accepted that the age model should not be largely affected by three points deviating from the general trend (35–36 cm, 75–76 cm and 145–146 cm).

To obtain the pollen composition and concentration 188 samples were analysed from the Lake Kotokel KTK10/6 core (Fig. 4). 60 pollen taxa and 70 non-pollen palynomorphs were identified (Müller et al., 2014).

2.2. Wavelet analysis of climatic changes in ocean and continental records

Wavelet analysis is particularly useful for non-stationary time series, which are dominated by periodicities that change with time (Debret et al., 2009). The advantage of wavelet analysis in detecting climatic periodicity was demonstrated on numerous climatic records to evaluate millennial and centennial cycles (Debret et al., 2009). We used the Morlet wavelet implemented in the Matlab code (Torrence and Compo, 1998). Monte Carlo simulation was used to assess the statistical significance of peaks in wavelet spectra. Resulting original data curves were detrended to remove the effect of the long-term climate changes usually related to the Milankovitch cyclicity. To calculate the trend we used the nonlinear locally weighted polynomial regression using weighted linear least squares and a 2nd degree polynomial model implemented in the Matlab functions "smooth" and "loess". The detrended data were resampled in regular intervals (10–40 yr) and normalized for the spectral analysis as $Normalized\ Parameter = \frac{Parameter - mean(Parameter)}{\sqrt{variance}}$ (Torrence and Compo, 1998). Background noise for each signal was estimated and separated using the singular spectrum analysis. Autoregressive (AR) modelling implemented in Torrence and Compo (1998), where AR (1) is red noise that is larger than zero, was used for each noise time series to determine the AR (1) stochastic process against which the initial time series was tested.

3. Results

Analyses of the pollen data and pollen-based biome allowed reconstructing the LGM environment in the region when steppe and tundra vegetation were composed mostly of grasses and various herbs (Bezrukova et al., 2010; Müller et al., 2014). The needleleaf coniferous and broadleaf deciduous tree and shrub taxa in our study are thinly distributed and typically presented between 2.4 and 5.4% of the total pollen concentration (TPC) (Fig. 4). The main component in the analysed TPC is the herbaceous pollen taxa. The most abundant grasses Poaceae (25–40%), sedges Cyperaceae (10–35%) and sagebrush Artemisia (10–40%) are typical for

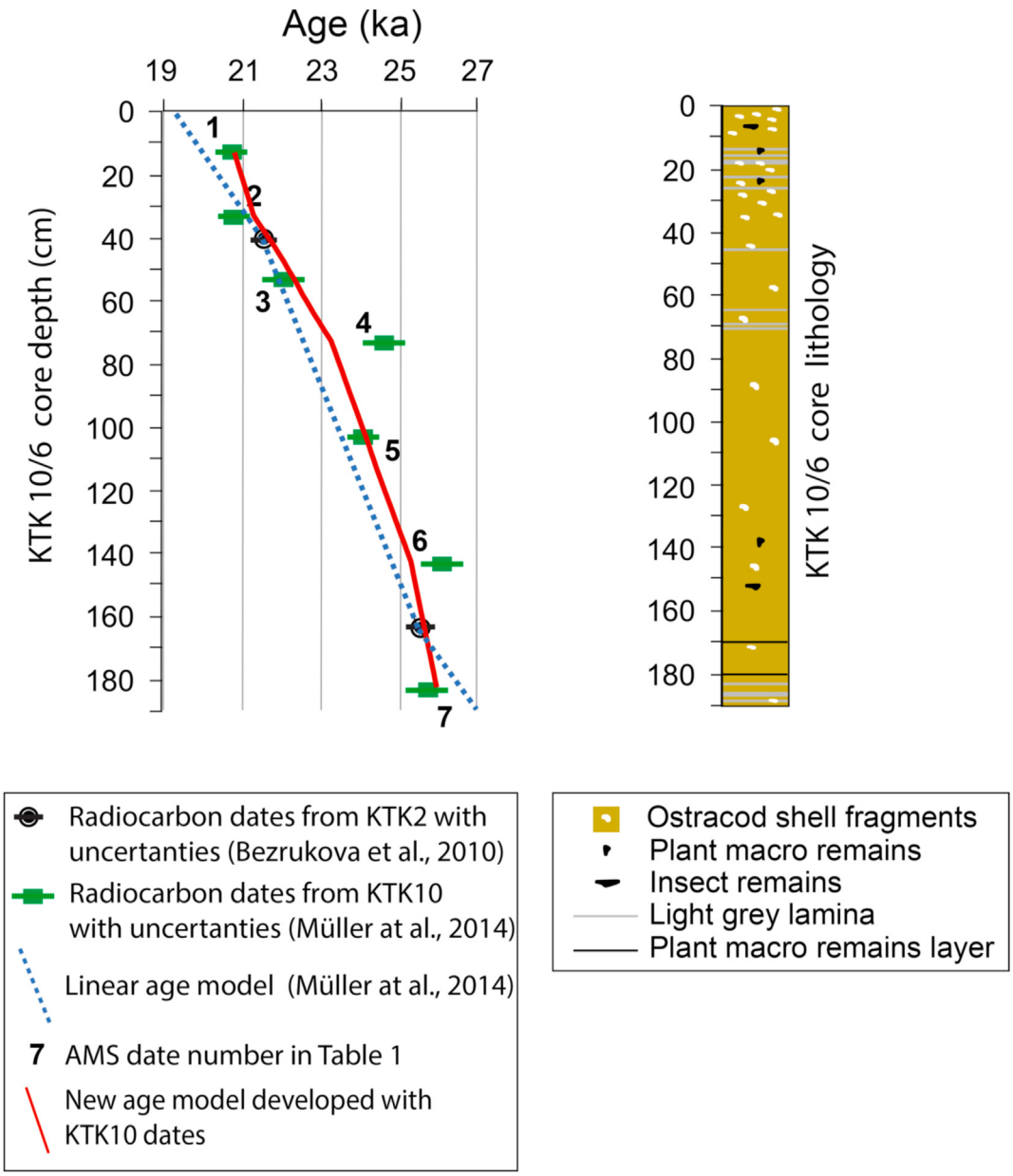

Fig. 2. Newly developed nonlinear age model for the Lake Kotokel core KTK10/6 (red line) using the Bayesian statistics approach (Blaauw and Christen, 2011) in comparison with previous linear age model (dotted blue line) for the cores KTK10/6 and KTK2 sampled at the same site (after Müller et al., 2014). (For interpretation of the references to colour in this figure legend, the reader is referred to the Web version of this article.)

Table 1
The AMS radiaocarbon dates from the Lake Kotokel sedimentary cores KTK10/6. Uncalibrated dates for the KTK10/6 samples were published in Müller et al. (2014). The ages were obtained in the Poznań Radiocarbon Laboratory, Poland, using bulk sediment. Calibrated age was obtained using the Bayesian statistics approach and software (Blaauw and Christen, 2011; Blaauw et al., 2018) applying the calibration curve IntCal20 (Reimer et al., 2020).

Number	Core	Depth (cm)	Sediment type	Uncalibrated age	Calibrated age (calendar years before present)
1	KTK10/6	15–16	Dark grey silty clay	17,230 ± 90	20,881 ± 298
2	KTK10/6	35–36	Dark grey silty clay	17,310 ± 90	21,370 ± 420
3	KTK10/6	55–56	Dark grey silty clay	18,410 ± 100	22,336 ± 265
4	KTK10/6	75–76	Dark grey silty clay	20,560 ± 120	23,278 ± 458
5	KTK10/6	105–106	Dark grey silty clay	20,120 ± 90	24,134 ± 268
6	KTK10/6	145–146	Dark grey silty clay	21,780 ± 110	25,246 ± 485
7	KTK10/6	185–186	Dark grey silty clay	21,590 ± 100	25,963 ± 269

herbaceous tundra and the steppe in the Lake Baikal area. The other grasses presented in smaller quantities are Asteraceae subfamily Cichorioideae (up to 8%), Caryophyllaceae (up to 6%), and Asteraceae subfamily Asteroideae (up to 6%) and Ranunculaceae (the

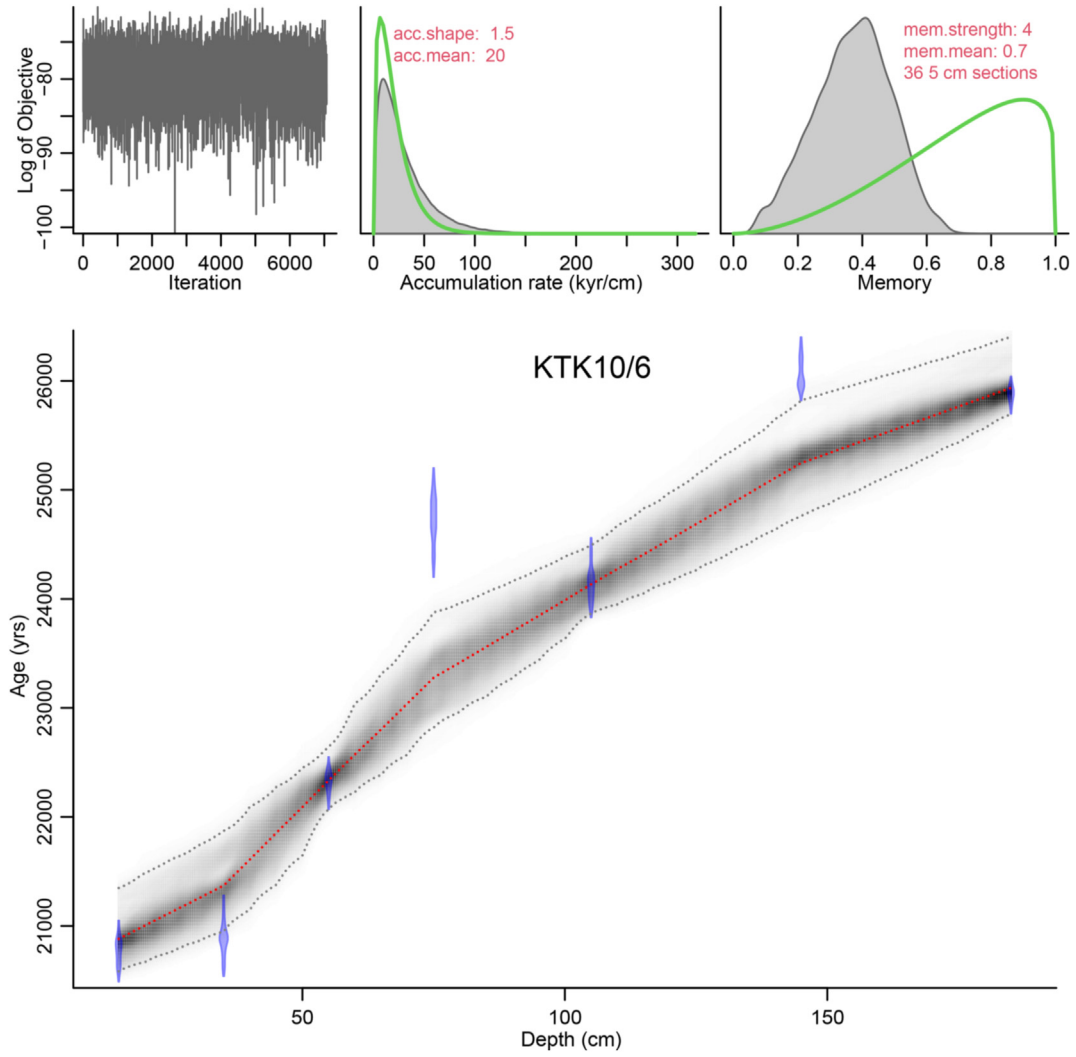

Fig. 3. The age model construction outcomes of the Bacon software (Blaauw and Christen, 2011). Top left panel shows Markov Chain Monte Carlo iteration number, and the distance from the objective (iterations stop when changes between interactions are small). Center top panel showing prior (green) and subsequent (grey shaded) histogram for sediment accumulation rate. Top right panel showing histograms for prior (green) and subsequent (grey shaded) memory, or autocorrelation. Main panel shows KTK age/depth input values (blue points), final age/depth relationship (dashed red line) and 95% confidence interval (shaded grey area). (For interpretation of the references to colour in this figure legend, the reader is referred to the Web version of this article.)

percentage varies largely in the core). The total pollen concentration averages at ~16 × 10^3 grains/g with alterations between ~4.75 × 10^3 and ~51 × 10^3 grains/g. Variations in the pollen composition do not indicate any abrupt changes in the core, which implies that the region surrounding Lake Kotokel was covered by relatively stable vegetation during the LGM (Müller et al., 2014). The Lake Kotokel fossil pollen concentration provides a reconstruction of vegetation and environments in continental Asia between 20.6 and 26 ka with temporal resolution of ~40 yr.

The total pollen concentration was a superposition of various pollen taxa in the record. The increase in the pollen concentration corresponded to the relatively warmer and wetter climate and linked to the increase in diatom concentration in the Lake Baikal, Lake Kotokel and the surrounding region (Tarasov et al., 2009; Bezrukova et al., 2010, 2011, 2011; Kostrova et al., 2016). The total pollen concentration (Fig. 4) acted as a stacked climatic parameter that smoothed the record but at the same time balanced out some uncertainties related to individual reaction of particular taxa to specific short-term conditions.

The grassland vegetation in the area was generally stable during this period, which would provide a persistent source of nourishment and a sustainable environment for large populations of herbivores, and consequently for local hunter-gatherers in the Lake Baikal region. Previous pollen and diatom analysis demonstrated that relatively wetter climate conditions corresponded to the less continental climate and relatively drier conditions corresponded to the cooler climate (Tarasov et al., 2009; Bezrukova et al., 2010, 2011, 2011; Kostrova et al., 2016). Wetter and warmer environment was characterized by general increase of vegetation on the shore that led to increase of the TPC values in our record. Fig. 5 illustrates the comparison of *Cyperaceae*, a type of plant that is associated with a wetter environment, and *Artemisia*, typical representative of steppe vegetation, i.e. drier environment. These two taxa demonstrated the inverted relationship indicating a relatively wetter vs. drier environment. We normalized and stacked together the two records for further spectral analysis in order to reduce any data uncertainty related to the lab measurements and field sampling. The stack is more sensitive to the moisture variations in the region comparing to the TPC that is sensitive for both temperature and moisture variations.

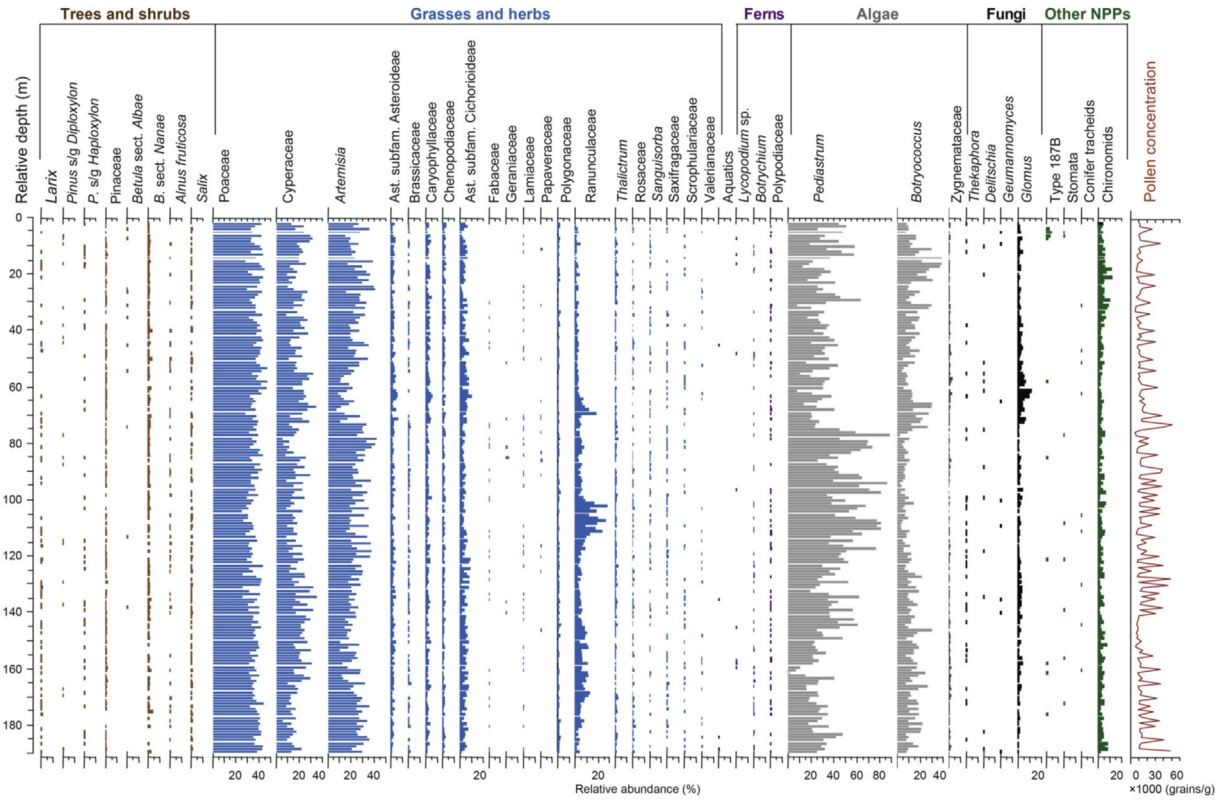

Fig. 4. Lake Kotokel pollen percentage diagram including percentages of the selected non-pollen palynomorphs (NPPs) (re-plotted after Müller et al., 2014).

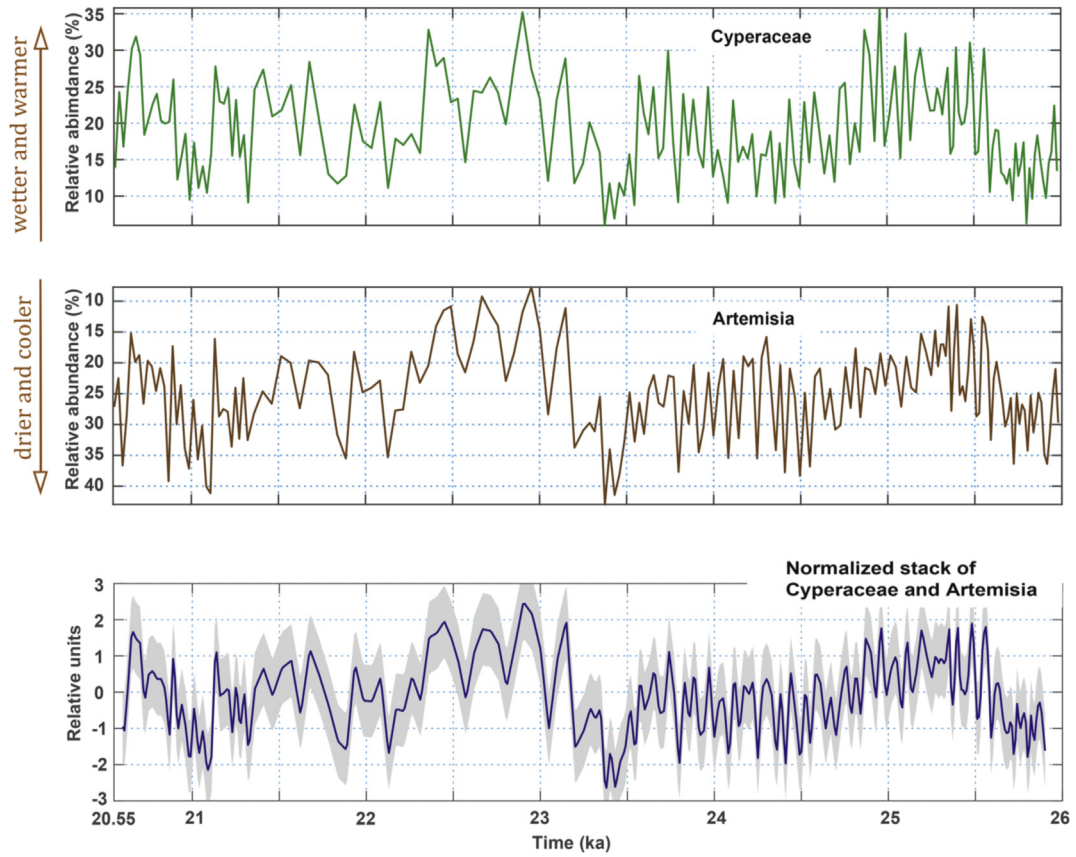

Fig. 5. Pollen percentage diagram for *Cyperaceae* and *Artemisia*. The stacked record of both taxa was normalized and detrended. The standard deviation shown in grey.

To explore whether the Lake Kotokel record corresponds to global climatic variations during the LGM we compared our total pollen record with the oxygen isotope $\delta^{18}O$ record from the Greenland ice core project (NGRIP) (Rasmussen et al., 2014), dust-fall contributions in Lake Qinghai in China (An et al., 2012), grain size at the Jingyuan and Gulang loess sections near Tengger Desert (Sun et al., 2012) and the composite oxygen isotope $\delta^{18}O$ record from the Alpine cave system 7H (Luetscher et al., 2015) (Fig. 1). The $\delta^{18}O$ NGRIP record (75.10° N, 42.32° W) has a resolution of 20 years and is accurately dated (Rasmussen et al., 2014) and has therefore it become a climatic reference curve for other paleoclimate records for worldwide comparison and especially for the Northern hemisphere (i.e., Moreno et al., 2014; Mingram et al., 2018). The NGRIP record revealed large millennial and centennial scale variability that is interpreted to be driven by the temperature changes (Kindler et al., 2014). The Alps are a barrier for meridional moisture transport and therefore record shifts in the North Atlantic storm track pattern is recorded in the Alpine cave system 7H (46°44′58″N, 7°48′28″E) (Luetscher et al., 2015).

The Lake Qinghai Westerlies climate index (dust flux of >0.25 μm fraction) is the only climate proxy record in Asia with a resolution (~20 yr) comparable to that of Lake Kotokel (~40 yr). Time series plots of the NGRIP oxygen isotope, the Lake Qinghai dust flux index, Gulang loess grain size, and the Lake Kotokel stack of *Cyperaceae* and *Artemisia* and pollen concentration records are presented in Fig. 6. The oxygen isotope record from Greenland demonstrates frequent low amplitude changes in average temperature, with the warmest interval at ~23.6 ka and a cooler climate between ~23.5 and 26 ka (Fig. 6a). Lake Qinghai (36°32′–37°15′ N, 99°36′–100°47′ E), the largest lake in China, is situated in the border area between the humid monsoon-dominated and the arid continental climate zones (An et al., 2012). The dominant arid climate during the LGM brought more dust during relatively cooler intervals. The high dust flux in the Lake Qinghai record corresponds to strong winds and a cool climate (Fig. 6b); therefore, the vertical axis in the Lake Qinghai figure is inverted relative to the NGRIP and Lake Kotokel records.

Loess deposits at Jingyuan (36.35° N, 104.60° E) and Gulang (37.49° N, 102.88° E) are situated in the depocentre of modern dust storms near Tengger Desert (Sun et al., 2012). High sedimentation rates and weak pedogenesis make these loess locations sensitive recorders of rapid monsoon changes where the sedimentary grain size primarily reflects changes in winter monsoon strength. The Gulang loess grain size shows higher amplitudes with abrupt transitions (Fig. 6c) and the Jingyuan loess has higher accumulation rates and coarser grain size with smoother amplitudes.

The stacked record of *Cyperaceae* and *Artemisia* is generally more sensitive for the wetter/drier climate variations (Fig. 6d), and pollen concentration increases during warm intervals and decreases when the climate conditions are cold (Fig. 6e). The pollen quantities reflect regional and local vegetation compositions around Lake Kotokel and vary with apparently larger amplitudes of cool and drier to warm and wetter climate compared to the $\delta^{18}O$ record from the Greenland ice. Since neither the pollen nor the other records are calibrated to temperature, it is unknown which has the larger amplitude temperature variations. It is also possible that the relationship between climate and the Lake Kotokel pollen concentration could be non-linear to some degree.

There is no striking visual correlation among the NGRIP oxygen isotopes, the Lake Qinghai dust flux, the Gulang loess grain size, and the Lake Kotokel pollen concentration in Fig. 6. Possible reasons for that include chronological uncertainties of the data, natural lags in global climate events (Clark et al., 2012), and ocean and continental feedback mechanisms that cause amplification of, or a lag in, particular events (Claussen et al., 2003). We applied thousands of various lags between the records in an iterative manner, but there was no significant improvement in the correlation coefficient. Therefore we plotted a trend line using the locally weighted linear least-squares regression "loess" implemented in Matlab to highlight the visuality of centennial and millennial duration features (black dashed lines in Fig. 6), where short events are smoothed out. Five to eight millennial length cycles can be visually identified in the records, although the peaks are shifted relative to each other suggesting different individual proxy responses to the centennial scale global climate change and/or age model imperfections.

To evaluate a common periodicity in the LGM climate we performed wavelet analyses (WA) on the Greenland ice core oxygen isotopes, the Lake Qinghai dust flux, the Lake Kotokel pollen time series, the stacked record of *Cyperaceae* and *Artemisia* (Fig. 7) and the composite oxygen isotope $\delta^{18}O$ record from the Alpine cave system 7H and the grain size in the Gulang and Jingyuan loess (Fig. 8). The WA highlights major features at the 95% confidence level; the most prominent cycle in the records is the ~1000-yr cycle throughout most of the LGM period. The ~1500 yr cycle in the Alpine cave system 7H reflects the North Atlantic storm track pattern that are similar to the circulation patterns in the Arctic Ocean and are not influenced by the solar forcing as suggested by Darby et al. (2012). The ~1000-yr peaks of the NGRIP, Lake Qinghai dust flux, Lake Kotokel TPC and Jingyuan loess records are distinct throughout the studied LGM interval with some modulations towards longer periods in the stacked record of *Cyperaceae* and *Artemisia*, composite oxygen isotope $\delta^{18}O$ record from the Alpine cave system and Gulang grain size records. Almost the same peak with the maximum at 900-yr can be traced in the Lake Kotokel pollen concentration wavelet analysis spectrum at 22.5–26 ka (Fig. 7c) when the millennial cycle amplitude variations are higher than for the interval 20.6–22.5 ka. The average spectral peak in the stacked record of *Cyperaceae* and *Artemisia* is centered at 1200-yr cycle (Fig. 7d). The difference with the 1000-kyr peak in other records could be driven by less sharp individual responses of these two types of plants to the humidity and temperature changes in the study region and/or sensitivity of these plants to other environmental factors or be related to a stronger temperature sensitivity of the total pollen concentration vs. a hydrological sensitivity of the Cyperaceae-Artemisia stack. Fig. 9 demonstrates the correspondence of the ~1000-yr peaks in the relatively smoothed *Cyperaceae* and *Artemisia* stack and the more detailed total pollen concentration record. Sensitivity of the *Cyperaceae* and *Artemisia* record to the variations of moisture, rather than temperature, may lead to the appearance of the cycles at periodicity of ~1200 kyr. The peaks in Fig. 9 are extracted from the whole record by applying the "loess" function that is a built-in Matlab script (see Methods). The millennial peaks 1 and 2 in the TPC record have low amplitude and are manifested by ~500 kyr cycles 1a, 1b, 2a and 2b in the pollen concentration record. The millennial cycles 3–6 have higher amplitudes and are therefore well pronounced in the WA in the interval 22.5–26 ka (Fig. 7c). The *Cyperaceae* and *Artemisia* stack has fewer peaks and manifests the smoothing of the response in comparison to the total pollen concentration record. Low amplitude peaks 1b and 2a are recorded as one low amplitude peak. The higher amplitude peaks 2b, 3a and 3b are registered as one high amplitude peak, the peak 4 appears in both records, and the pollen concentration peaks 5 and 6 appear as one peak in the stack. The stack still demonstrates confidently that millennial scale cycles

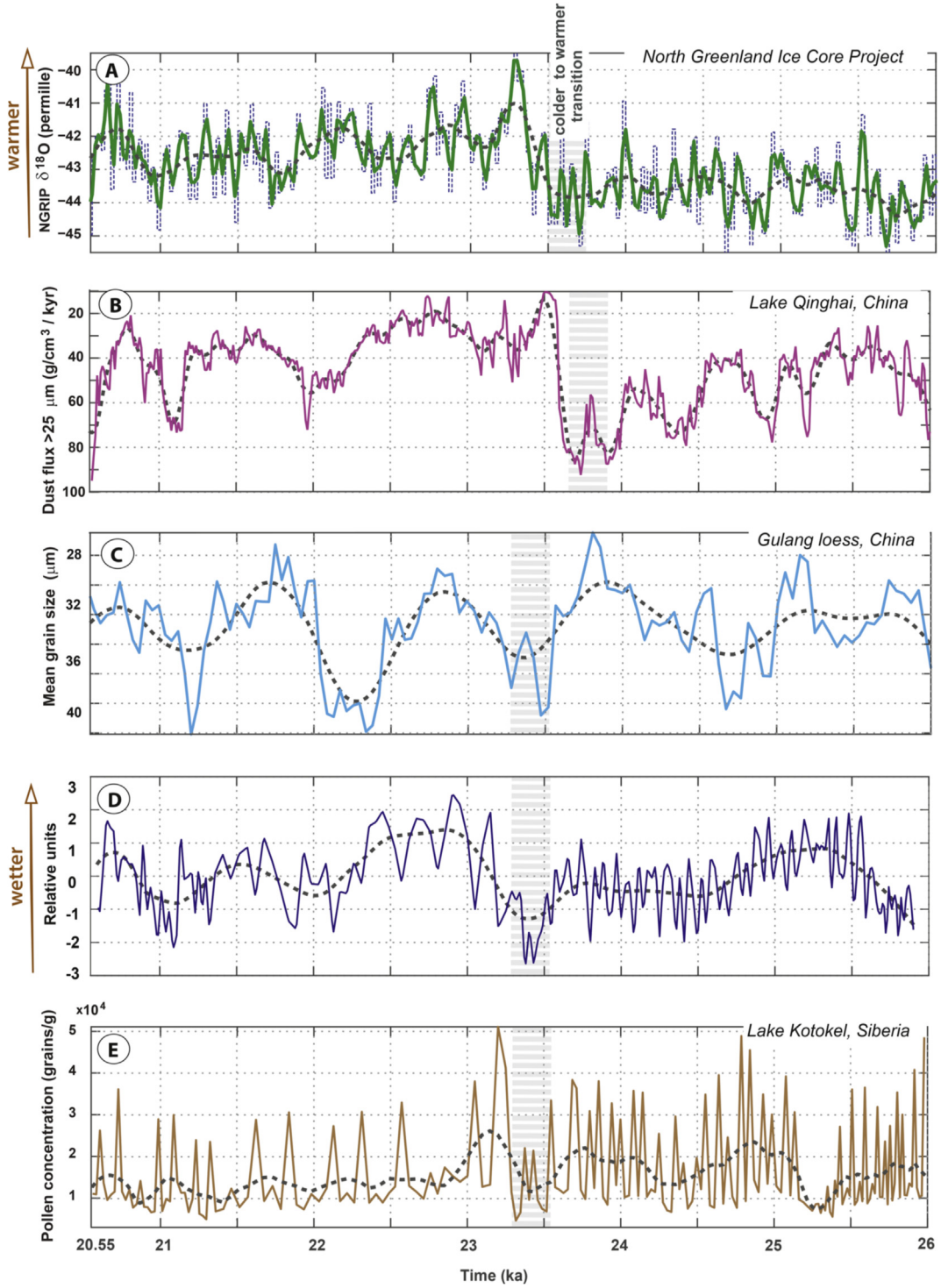

Fig. 6. Comparisons among (A) the NGRIP oxygen isotope $\delta^{18}O$ from Greenland (Rasmussen et al., 2014), (B) the Lake Qinghai dust flux Westerlies climate index (dust flux of >0.25 μm fraction) (An et al., 2012) (note inverted vertical axis), (C) the grain size of the Gulang loess, China (Sun et al., 2012), (D) the stack of *Cyperaceae* and *Artemisia* (this study) and (E) the total pollen concentration in samples from Lake Kotokel (this study). Thin dashed blue lines are original data; green, magenta, blue and brown solid lines represent data that have been smoothed and resampled into equally spaced intervals; the thick dashed grey line is smoothed data, calculated using Matlab function "loess" weighting 5–10% of the whole data set, to visualize the centennial and millennial periodicity. (For interpretation of the references to colour in this figure legend, the reader is referred to the Web version of this article.)

exist in the record, however, the smoothing character of the *Cyperaceae* and *Artemisia* record cannot be used for accurate extraction of the individual cycles. The total pollen concentration recorded is the better recorder of the centennial scale climate cyclicity in Lake Kotokel.

Fundamental centennial scale solar modes at periodicities of 1000-yr and 500-yr, plus additional periodicities of ~700-yr and ~300-yr of an uncertain nature, are identified in the Holocene (Soon

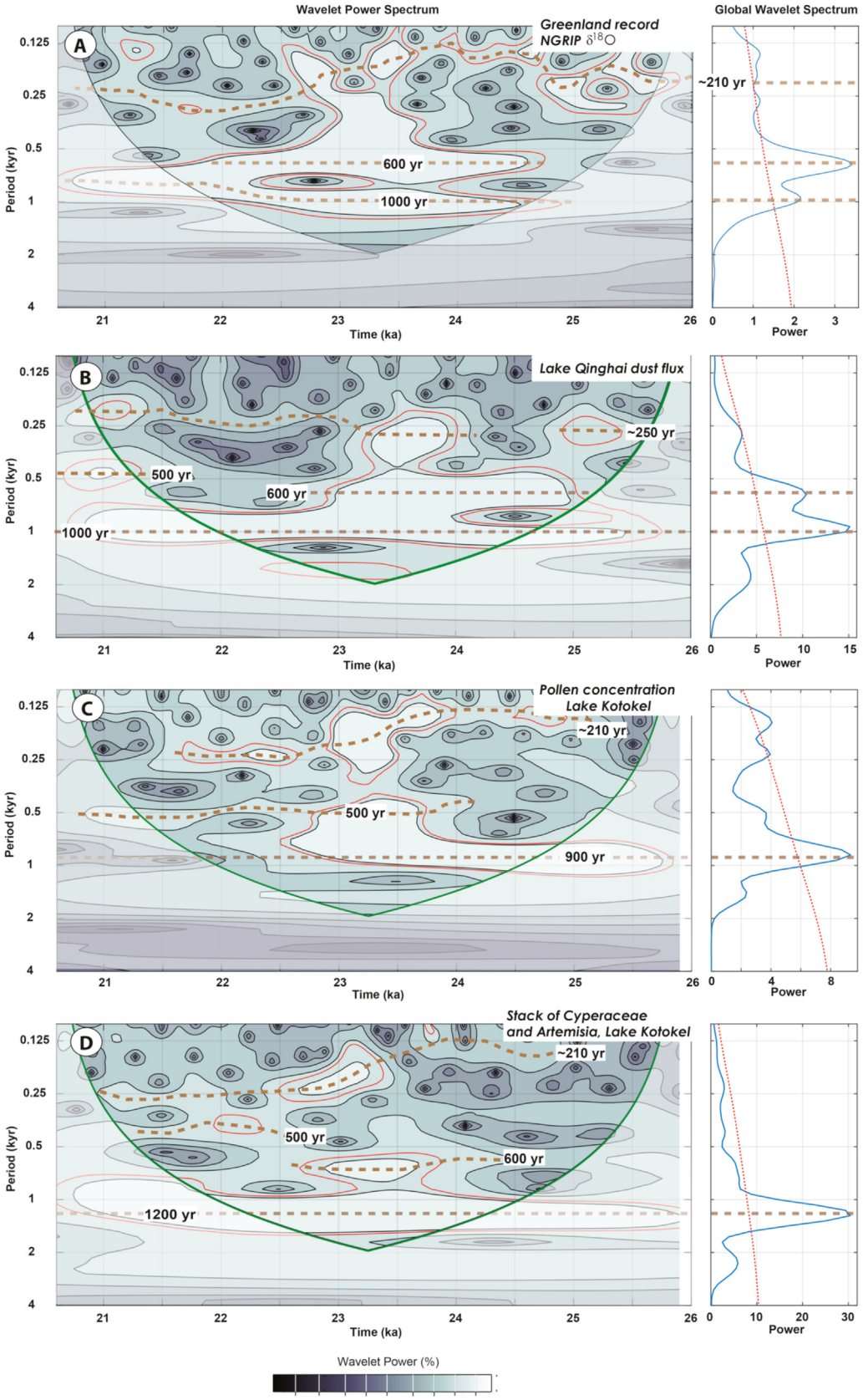

Fig. 7. Wavelet transform analyses of the 20.6–26 ka interval for the NGRIP oxygen isotope from Greenland (Rasmussen et al., 2014), the Lake Qinghai dust flux Westerlies climate index (An et al., 2012), the total pollen concentration in samples and stacked record of *Cyperaceae* and *Artemisia* from Lake Kotokel. Dashed horizontal lines represent 1000-, 500-, and 250-yr periods. Darker shaded cone shaped areas correspond to cones of influence; the green cone line is the 95% confidence spectrum. Confidence levels of more than 95% are indicated with a red line. Fourier power spectra of the parameters are in separate figures at the right of the main diagrams; the red dashed line is the mean red noise spectrum. (For interpretation of the references to colour in this figure legend, the reader is referred to the Web version of this article.)

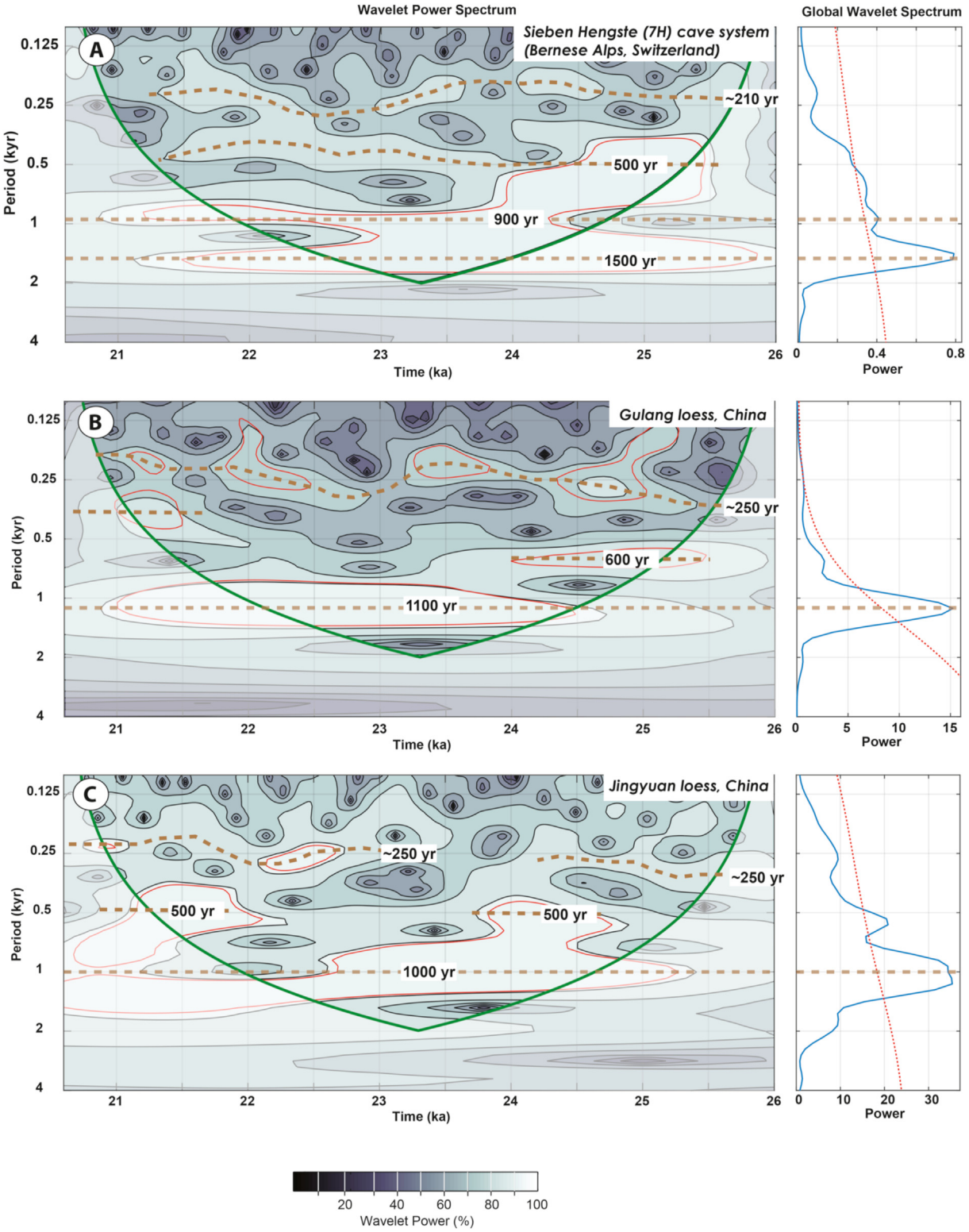

Fig. 8. Wavelet transform analyses of the 20.6–26 ka interval for the composite oxygen isotope $\delta^{18}O$ record from the Alpine cave system 7H (Luetscher et al., 2015) and the grain size at the Jingyuan and Gulang loess sections near Tengger Desert (Sun et al., 2012). Dashed horizontal lines represent 1000-, 500-, and 250-yr periods. Darker shaded cone shaped areas correspond to cones of influence; the green cone line is the 95% confidence spectrum. Confidence levels of more than 95% are indicated with a red line. Fourier power spectra of the parameters are in separate figures at the right of the main diagrams; the red dashed line is the mean red noise spectrum. (For interpretation of the references to colour in this figure legend, the reader is referred to the Web version of this article.)

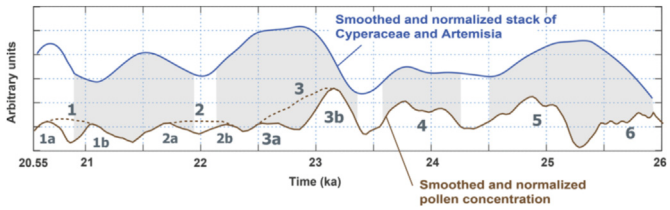

Fig. 9. Comparison of centennial and millennial scale cycles for the smoothed and normalized stack of the pollen percentage for *Cyperaceae* and *Artemisia* plants stack and total pollen concentration. Some of the peaks well pronounced in the total pollen concentration are much smoothed and therefore hidden in the stack illustrating that the total pollen concentration record is a better proxy of the centennial scale climate cyclicity.

et al., 2014). The LGM spectra in Figs. 6 and 7 indicate the presence of relatively weak cycles at ~500-600-yr and ~210-250-yr in all records, which appear at different time intervals. These cycles have weaker amplitudes compared to the 1000–1500 yr cycle in the climate proxy records and sun spot number in the Holocene (Kravchinsky et al., 2013). The 500–600 cycle could be a harmonic or a modulation of other cycles and it might not be compared exactly between each record considering the age model uncertainty in available records. At the same time, we may confidently report its presence in all the records discussed here. The ~210–250 cycle corresponds well to the de Vries cycle confidently observed in the Holocene (Steinhilber et al., 2012).

4. Discussion

The most prominent ~1000-yr and ~500-600-yr climate periodicity found in the Lake Kotokel pollen record during the LGM has been already reported in Holocene climatic series of the studied Lake Baikal region, in the insolation variance, and sunspot number (Kravchinsky et al., 2013). The Siberian Holocene loess-soil Burdukovo site is close to the Lake Kotokel core site (Fig. 1). Both sections are situated in the Lake Baikal region of Siberia and are remote from the ocean. The Holocene spectrum is coherent in both sunspot number and solar modulation spectra at the statistically significant peaks of 1000 and 500 years (Fig. 10 from Kravchinsky et al., 2013).

A large number of Holocene climatic proxies from the North Atlantic Ocean, the Western Pacific Ocean, the Southern (Antarctic) Ocean, and the East Asian monsoon regions show fundamental periodicities of 2300, 1000, and 500 yr (Soon et al., 2014), where 1000 and 500 yr cycles are identical to the periodicities in the LGM reported here. The strong 1000-yr peak in the Holocene spectrum matched the cosmogenic ^{10}Be and especially ^{14}C records from Northern Atlantic cores (Debret et al., 2009). The concentration of these isotopes depends on solar radiation and the strength of the Earth's magnetic field, and can therefore be expected to show similarity to the sunspot number and solar insolation variation spectra on the centennial time scale in the Holocene. The power spectrum of tree pollen concentration in the Lake Xiaolongwan sediments in Eastern Asia showed ~500-yr periodicity during the middle-late Holocene that was interpreted to be linked to the Greenland temperature change. The spectral analysis of the solar activity reconstructed from the ^{14}C from the tree ring worldwide records and ^{10}Be records from the ice core of the European Project for Ice Coring in Antarctica revealed statistically significant periodicities at ~210 yr (de Vries cycle), ~350 yr (unnamed cycle), and ~1000 yr (the Eddy cycle) in the last 9400 yrs (Steinhilber et al., 2012). They also reported less significant unnamed cycles at ~500 and ~710 yrs. Such periodicities are reported in the Asian climate (Wang et al., 2005) and sunspot number (Kravchinsky et al., 2013) during the Holocene. The Lake Kotokel TPC carries 500–600 yr periodicity similarly to these Holocene records.

Another prominent cycle in the Lake Kotokel record is centered at ~210-250-yr. It was suggested that the periodicity at 300-yr may hypothetically correspond to responses of the Atlantic thermohaline circulation to external solar modulation and pacing, but the exact reason is not known (Soon et al., 2014). The cross-wavelet analyses of a late Holocene speleothem record from Dongge Cave in China showed statistically strong coherence similar to our study periodicities (200 and 340 yrs) suggesting that solar activities modulate Asian monsoon changes. Such periodicity is close to the ~210-250-yr cycle reported here for the LGM. The presence of the ~210 yr de Vries cycle in the ^{10}Be data from the GRIP ice core from Greenland was demonstrated between 50 and 25 ka (Wagner et al., 2001) and between 22.5 and 10 ka (Adolphi et al., 2014). The age model for the GRIP core, however, was re-evaluated and synchronized to the NGRIP record later (Rasmussen et al., 2014). Nevertheless our WA analysis shows the presence of the cycle in the latest version of the oxygen isotope record of NGRIP (Fig. 7a).

The short-term variations of the Earth's motion around the Sun over the last 6000 years using 1-yr steps demonstrated that the main centennial scale climate periodicities related to the Earth's motion should be at 250-yr (eccentricity and obliquity) and at ~1000-yr (840-yr obliquity and precession and 930-yr eccentricity) (Loutre et al., 1992). The authors concluded that while precession dominates at any latitude, the obliquity signal is stronger at high latitudes, making the 250-yr signal an important periodicity for climate research, although such changes cause additional amplitude changes in solar insolation of ~0.2 Wm^{-2} at the maximum (Soon et al., 2014). The ~210-250-yr cycle can be clearly identified in the pollen record of Lake Kotokel (Fig. 7c and d), suggesting that the precession and eccentricity components (Loutre et al., 1992) could also potentially contribute to the solar mode variations. At the same time, it has been widely discussed that a change of 1.5–2 W/m^2 in the Holocene solar radiation cannot explain the direct influence of solar variability on climate change without additional and still debated feedback mechanisms (Usoskin et al., 2007). It was shown that the most prominent temporal features of the solar dynamo, including the de Vries cycle, can be explained by combined synchronization with tidal forcing of the Venus–Earth–Jupiter system and the periodic motion of the Sun around the barycenter of the solar system (Stefani et al., 2021). The simulations of the Bond cycles before the Holocene suggested that it is possible that the solar cyclicity is driven by a stochastic process and therefore quasi-periodic (Stefani *et al.*, 2021). In contrast, other climate modeling and observation data in the Holocene suggest that solar forcing may trigger surface temperature variability and atmospheric dynamics via changes in cloud formation (Gray et al., 2010; Solanki et al., 2013), although a robust link between cosmic rays and cloud cover is not confirmed (Voiculescu and Usoskin, 2012). The review of suggested mechanisms that link solar variability and climate change is provided in Solanki et al. (2013). Although the mechanisms behind the centennial periodicities are still actively debated in the literature, our study demonstrates that the LGM climate proxy records from different regions are characterized by the cycles of comparable duration.

5. Conclusions

Highlighted by our spectral analysis similarities between Holocene and LGM climate oscillations in the deep continental interior of Asia, thousands of kilometres away from oceanic influence, and in Greenland and Alpine regions suggest that fundamental periodicities in glacial climate conditions and in models describing centennial solar activity can be extrapolated from the Holocene back in time to the LGM. Our findings suggest that such

periodicities are a lasting attribute of climate change. The climate variations at ~1000, 500–600 and 210-250-yr were proposed to be linked to the variations of the amount of solar input to the Earth. Such variations may have always been an existing factor of the global climate dynamics in the geological past in addition to widely accepted Milankovitch cycles of much longer periods.

Declaration of competing interest

The authors declare that they have no known competing financial interests or personal relationships that could have appeared to influence the work reported in this paper.

Acknowledgments

We thank Z. An for sharing the data for the Lake Qinghai and Y. Sun for sharing the data for the Gulang and Jingyuan loess sections. The manuscript greatly benefited from suggestions of W. Fletcher, C. O'Cofaigh and C. Hillaire-Marcel. This study was funded by the Natural Sciences and Engineering Research Council of Canada (NSERC grant RGPIN-2019-04780) for V.A.K.

Author contributions

All authors have made substantial contributions to a submission. V.A.K. and P.E.T. conceived the idea of this study, V.A.K., R.Z. and R.B. wrote the manuscript, V.A.K., R.Z., R.B. and T.A. performed data analysis and prepared the figures, S.M. measured and analysed the pollen content, P.E.T., M.V.B. and A.G. contributed to discussions of the materials and results and to numerical analysis.

Data availability

We release the Lake Kotokel supplementary data presented here to the public domain at https://zenodo.org/record/5204415.

Appendix A. Supplementary data

Supplementary data to this article can be found online at https://doi.org/10.1016/j.quascirev.2021.107171.

References

Adolphi, F., Muscheler, R., Svensson, A., Aldahan, A., Possnert, G., Beer, J., Sjolte, J., Björck, S., Matthes, K., Thieblemont, R., 2014. Persistent link between solar activity and Greenland climate during the Last Glacial Maximum. Nat. Geosci. 7 (9), 662–666.

An, Z., Colman, S.M., Zhou, W., Li, X., Brown, E.T., Jull, A.T., Cai, Y., Huang, Y., Lu, X., Chang, H., Song, Y., 2012. Interplay between the Westerlies and asian monsoon recorded in Lake Qinghai sediments since 32 ka. Sci. Rep. 2, 619.

Bezrukova, E.V., Krivonogov, S.K., Takahara, H., Letunova, P.P., Shichi, K., Abzaeva, A.A., Kulagina, N.V., Zabelina, Y.S., 2008. Lake Kotokel as a stratotype for the late glacial and Holocene in southeastern Siberia. Dokl. Earth Sci. 420 (1), 658–663.

Bezrukova, E.V., Tarasov, P.E., Solovieva, N., Krivonogov, S.K., Riedel, F., 2010. Last glacial-interglacial vegetation and environmental dynamics in southern Siberia: chronology, forcing and feedbacks. Palaeogeogr. Palaeoclimatol. Palaeoecol. 296, 185–198.

Bezrukova, E.V., Tarasov, P.E., Kulagina, N.V., Abzaeva, A.A., Letunova, P.P., Kostrova, S.S., 2011. Palynological study of Lake Kotokel' bottom sediments (Lake Baikal region). Russ. Geol. Geophys. 52 (4), 458–465.

Bianchi, G.G., McCave, I.N., 1999. Holocene periodicity in North Atlantic climate and deep-ocean flow south of Iceland. Nature 397, 515–517.

Blaauw, M., Christen, J.A., 2011. Flexible paleoclimate age-depth models using an autoregressive gamma process. Bayesian analysis 6 (3), 457–474.

Blaauw, M., Christen, J.A., Bennett, K.D., Reimer, P.J., 2018. Double the dates and go for Bayes—impacts of model choice, dating density and quality on chronologies. Quat. Sci. Rev. 188, 58–66.

Bond, G., Showers, W., Cheseby, M., Lotti, R., Almasi, P., Priore, P., Cullen, H., Hajdas, I., Bonani, G., 1997. A pervasive millennial-scale cycle in North Atlantic Holocene and glacial climates. Science 278 (5341), 1257–1266.

Bond, G.C., Showers, W., Elliot, M., Evans, M., Lotti, R., Hajdas, I., Bonani, G., Johnson, S., 1999. The North Atlantic's 1–2 kyr climate rhythm: relation to Heinrich events, Dansgaard/Oeschger cycles and the little ice age. In: Clark, P.U., Webb, R.S., Keigwin, L.D. (Eds.), Mechanisms of Global Change at Millennial Time Scales. Geophysical Monograph, American Geophysical Union, Washington DC, pp. 59–76.

Clark, P.U., Dyke, A.S., Shakun, J.D., Carlson, A.E., Clark, J., Wohlfarth, B., Mitrovica, J.X., Hostetler, S.W., McCabe, A.M., 2009. The last glacial maximum. Science 325 (5941), 710–714.

Clark, P.U., Shakun, J.D., Baker, P.A., Bartlein, P.J., Brewer, S., Brook, E., Carlson, A.E., Cheng, H., Kaufman, D.S., Liu, Z., Marchitto, T.M., 2012. Global climate evolution during the last deglaciation. Proc. Natl. Acad. Sci. Unit. States Am. 109 (19), E1134–E1142.

Claussen, M., Ganopolski, A., Brovkin, V., Gerstengarbe, F.W., Werner, P., 2003. Simulated global-scale response of the climate system to Dansgaard/Oeschger and Heinrich events. Clim. Dynam. 21 (5–6), 361–370.

Darby, D.A., Ortiz, J.D., Grosch, C.E., Lund, S.P., 2012. 1,500-year cycle in the Arctic Oscillation identified in Holocene Arctic sea-ice drift. Nat. Geosci. 5 (12), 897–900.

Debret, M., Sebag, D., Crosta, X., Massei, N., Petit, J.R., Chapron, E., Bout-Roumazeilles, V., 2009. Evidence from wavelet analysis for a mid-Holocene transition in global climate forcing. Quat. Sci. Rev. 28, 2675–2688.

Dima, M., Lohmann, G., 2009. Conceptual model for millennial climate variability: a possible combined solar-thermohaline circulation origin for the ~ 1,500-year cycle. Clim. Dynam. 32 (2), 301–311.

Ditlevsen, P.D., Andersen, K.K., Svensson, A., 2007. The DO-climate events are probably noise induced: statistical investigation of the claimed 1470 years cycle. Clim. Past 3 (1), 129–134.

Gong, D.Y., Wang, S.W., Zhu, J.H., 2001. East Asian winter monsoon and Arctic oscillation. Geophys. Res. Lett. 28 (10), 2073–2076.

Gray, L.J., Beer, J., Geller, M., Haigh, J.D., Lockwood, M., Matthes, K., Cubasch, U., Fleitmann, D., Harrison, G., Hood, L., Luterbacher, J., 2010. Solar influences on climate. Rev. Geophys. 48 (4).

Grootes, P.M., Stuiver, M., 1997. Oxygen 18/16 variability in Greenland snow and ice with 10−3 to 105 year time resolution. J. Geophys. Res.: Oceans 102 (C12), 26455–26470.

Kaufman, D., McKay, N., Routson, C., Erb, M., Davis, B., Heiri, O., Jaccard, S., Tierney, J., Dätwyler, C., Axford, Y., Brussel, T., 2020. A global database of Holocene paleotemperature records. Scientific data 7 (1), 1–34.

Kindler, P., Guillevic, M., Baumgartner, M., Schwander, J., Landais, A., Leuenberger, M., 2014. Temperature reconstruction from 10 to 120 kyr b2k from the NGRIP ice core. Clim. Past 10 (2), 887–902.

Kostrova, S.S., Meyer, H., Tarasov, P.E., Bezrukova, E.V., Chapligin, B., Kossler, A., Pavlova, L.A., Kuzmin, M.I., 2016. Oxygen isotope composition of diatoms from sediments of Lake Kotokel (Buryatia). Russ. Geol. Geophys. 57 (8), 1239–1247.

Kravchinsky, V.A., Langereis, C.G., Walker, S.D., Dlusskiy, K.G., White, D., 2013. Discovery of Holocene millennial climate cycles in the Asian continental interior: has the sun been governing the continental climate? Global Planet. Change 110, 386–396.

Loehle, C., Singer, S.F., 2010. Holocene temperature records show millennial-scale periodicity. Can. J. Earth Sci. 47, 1327–1336.

Long, J.A., Stoy, P.C., 2013. Quantifying the periodicity of Heinrich and Dansgaard-Oeschger events during marine oxygen isotope stage 3. Quat. Res. 79 (3), 413–423.

Loutre, M.F., Berger, A., Bretagnon, P., Blanc, P.-L., 1992. Astronomical frequencies for climate research at the decadal to century time scale. Clim. Dynam. 7, 181–194.

Luetscher, M., Boch, R., Sodemann, H., Spötl, C., Cheng, H., Edwards, R.L., Frisia, S., Hof, F., Müller, W., 2015. North Atlantic storm track changes during the last glacial maximum recorded by alpine speleothems. Nat. Commun. 6, 6344.

Marsicek, J., Shuman, B.N., Bartlein, P.J., Shafer, S.L., Brewer, S., 2018. Reconciling divergent trends and millennial variations in Holocene temperatures. Nature 554 (7690), 92.

Martin-Puertas, C., Matthes, K., Brauer, A., Muscheler, R., Hansen, F., Petrick, C., Aldahan, A., Possnert, G., Van Geel, B., 2012. Regional atmospheric circulation shifts induced by a grand solar minimum. Nat. Geosci. 5 (6), 397–401.

McMichael, A.J., 2012. Insights from past millennia into climatic impacts on human health and survival. Proc. Natl. Acad. Sci. Unit. States Am. 109 (13), 4730–4737.

Mingram, J., Stebich, M., Schettler, G., Hu, Y., Rioual, P., Nowaczyk, N., Dulski, P., You, H., Opitz, S., Liu, Q., Liu, J., 2018. Millennial-scale East Asian monsoon variability of the last glacial deduced from annually laminated sediments from Lake Sihailongwan, NE China. Quat. Sci. Rev. 201, 57–76.

Moreno, A., Svensson, A., Brooks, S.J., Connor, S., Engels, S., Fletcher, W., Genty, D., Heiri, O., Labuhn, I., Perşoiu, A., Peyron, O., 2014. A compilation of Western European terrestrial records 60–8 ka BP: towards an understanding of latitudinal climatic gradients. Quat. Sci. Rev. 106, 167–185.

Müller, S., Tarasov, P.E., Hoelzmann, P., Bezrukova, E.V., Kossler, A., Krivonogov, S.K., 2014. Stable vegetation and environmental conditions during the last glacial maximum: new results from Lake Kotokel (Lake Baikal region, southern Siberia, Russia). Quat. Int. 348, 14–24.

Panagiotopoulos, F., Shahgedanova, M., Hannachi, A., Stephenson, D.B., 2005. Observed trends and teleconnections of the Siberian high: a recently declining center of action. J. Clim. 18 (9), 1411–1422.

Peavoy, D., Franzke, C., 2010. Bayesian analysis of rapid climate change during the last glacial using Greenland δ18 O data. Clim. Past 6, 787–794.

Pisias, N.G., Clark, P.U., Brook, E.J., 2010. Modes of global climate variability during marine isotope stage 3 (60–26 ka). J. Clim. 23 (6), 1581–1588.
Rahmstorf, S., 2003. Timing of abrupt climate change: a precise clock. Geophys. Res. Lett. 30 (10), 1510.
Rasmussen, S.O., Bigler, M., Blockley, S.P., Blunier, T., Buchardt, S.L., Clausen, H.B., Cvijanovic, I., Dahl-Jensen, D., Johnsen, S.J., Fischer, H., Gkinis, V., 2014. A stratigraphic framework for abrupt climatic changes during the Last Glacial period based on three synchronized Greenland ice-core records: refining and extending the INTIMATE event stratigraphy. Quat. Sci. Rev. 106, 14–28.
Reimer, P.J., Austin, W.E., Bard, E., Bayliss, A., Blackwell, P.G., Ramsey, C.B., Butzin, M., Cheng, H., Edwards, R.L., Friedrich, M., Grootes, P.M., 2020. The IntCal20 Northern Hemisphere radiocarbon age calibration curve (0–55 cal kBP). Radiocarbon 62 (4), 725–757.
Scafetta, N., Milani, F., Bianchini, A., Ortolani, S., 2016. On the astronomical origin of the Hallstatt oscillation found in radiocarbon and climate records throughout the Holocene. Earth Sci. Rev. 162, 24–43.
Schulz, M., 2002. On the 1470-year pacing of Dansgaard-Oeschger warm events. Paleoceanography 17 (2), 4-1.
Shichi, K., Takahara, H., Krivonogov, S.K., Bezrukova, E.V., Kashiwaya, K., Takehara, A., Nakamura, T., 2009. Late pleistocene and Holocene vegetation and climate records from Lake Kotokel, central baikal region. Quat. Int. 205 (1–2), 98–110.
Solanki, S.K., Krivova, N.A., Haigh, J.D., 2013. Solar irradiance variability and climate. Annu. Rev. Astron. Astrophys. 51, 311–351.
Solotchin, P.A., Solotchina, E.P., Bezrukova, E.V., Zhdanova, A.N., 2020. Climate signals in the late quaternary bottom sediments of lake baunt (Northern Transbaikalia). Russ. Geol. Geophys. 61 (10), 1146–1155.
Soon, W., Herrera, V.M.V., Selvaraj, K., Traversi, R., Usoskin, I., Chen, C.T.A., Lou, J.Y., Kao, S.J., Carter, R.M., Pipin, V., Severi, M., 2014. A review of Holocene solar-linked climatic variation on centennial to millennial timescales: physical processes, interpretative frameworks and a new multiple cross-wavelet transform algorithm. Earth Sci. Rev. 134, 1–15.
Sorrel, P., Debret, M., Billeaud, I., Jaccard, S.L., McManus, J.F., Tessier, B., 2012. Persistent non-solar forcing of Holocene storm dynamics in coastal sedimentary archives. Nat. Geosci. 5 (12), 892–896.
Stefani, F, Stepanov, R, Weier, T, 2021. Shaken and Stirred: When Bond Meets Suess–de Vries and Gnevyshev–Ohl. Solar Physics 296 (6), 1–23.
Steinhilber, F., Abreu, J.A., Beer, J., Brunner, I., Christl, M., Fischer, H., Heikkilä, U., Kubik, P.W., Mann, M., McCracken, K.G., Miller, H., 2012. 9,400 years of cosmic radiation and solar activity from ice cores and tree rings. Proc. Natl. Acad. Sci. Unit. States Am. 109 (16), 5967–5971.
Sun, Y., Clemens, S.C., Morrill, C., Lin, X., Wang, X., An, Z., 2012. Influence of Atlantic meridional overturning circulation on the East Asian winter monsoon. Nat. Geosci. 5 (1), 46.
Tarasov, P., Granoszewski, W., Bezrukova, E., Brewer, S., Nita, M., Abzaeva, A., Oberhänsli, H., 2005. Quantitative reconstruction of the last interglacial vegetation and climate based on the pollen record from Lake Baikal, Russia. Clim. Dynam. 25 (6), 625–637.
Tarasov, P.E., Bezrukova, E.V., Krivonogov, S.K., 2009. Late Glacial and Holocene changes in vegetation cover and climate in southern Siberia derived from a 15 kyr long pollen record from Lake Kotokel. Clim. Past 5 (3), 285–295.
Torrence, C., Compo, G.P., 1998. A practical guide to wavelet analysis. Bull. Am. Meteorol. Soc. 79 (1), 61–78.
Usoskin, I.G., Solanki, S.K., Kovaltsov, G.A., 2007. Grand minima and maxima of solar activity: new observational constraints. Astron. Astrophys. 471, 301–309.
Voiculescu, M., Usoskin, I., 2012. Persistent solar signatures in cloud cover: spatial and temporal analysis. Environ. Res. Lett. 7 (4), 044004.
Vonmoos, M., Beer, J., Muscheler, R., 2006. Large variations in Holocene solar activity: constraints from 10Be in the Greenland ice core project ice core. J. Geophys. Res.: Space Physics 111 (A10).
Wagner, G, Beer, J, Masarik, J, Muscheler, R, Kubik W, P, Mende, W, Laj, C, Raisbeck M, G, Yiou, F, 2001. Presence of the solar de Vries cycle (~ 205 years) during the last ice age. Geophys. Res. Lett. 28 (3), 303–306.
Wang, Y., Cheng, H., Edwards, R.L., He, Y., Kong, X., An, Z., Wu, J., Kelly, M.J., Dykoski, C.A., Li, X., 2005. The Holocene Asian monsoon: links to solar changes and North Atlantic climate. Science 308 (5723), 854–857.
Wanner, H., Beer, J., Bütikofer, J., Crowley, T.J., Cubasch, U., Flückiger, J., Goosse, H., Grosjean, M., Joos, F., Kaplan, J.O., Küttel, M., 2008. Mid-to Late Holocene climate change: an overview. Quat. Sci. Rev. 27 (19–20), 1791–1828.
Wunsch, C., 2000. On sharp spectral lines in the climate record and the millennial peak. Paleoceanography 15 (4), 417–424.